# Plasmonic Airy Beam Generated by In-Plane Diffraction

L. Li, T. Li,* S. M. Wang, C. Zhang, and S. N. Zhu

*National Laboratory of Solid State Microstructures, College of Physics, College of Engineering and Applied Sciences, Nanjing University†, Nanjing 210093, China*

(Received 14 July 2011; revised manuscript received 23 August 2011; published 15 September 2011)

We report an experimental realization of a plasmonic Airy beam, which is generated thoroughly on a silver surface. With a carefully designed nanoarray structure, such Airy beams come into being from an in-plane propagating surface plasmon polariton wave, exhibiting nonspreading, self-bending, and self-healing properties. Besides, a new phase-tuning method based on nonperfectly matched diffraction processes is proposed to generate and modulate the beam almost at will. This unique plasmonic Airy beam as well as the generation method would significantly promote the evolutions in in-plane surface plasmon polariton manipulations and indicate potential applications in lab-on-chip photonic integrations.

DOI: 10.1103/PhysRevLett.107.126804 PACS numbers: 73.20.Mf, 42.25.Fx, 78.67.−n

The Airy wave packet is the only nontrivial one-dimensional (1D) solution for a wave propagation maintaining the nonspreading property, which was deduced from the Schrödinger equation in quantum mechanics for a free particle [1]. Since its recent observation in optics [2], intensive studies have been carried out, such as self-accelerating [3], ballistic dynamics [4], and self-healing [5,6], as well as the recent nonlinear generation [7] and possible applications [8–10]. To date, most of these optical Airy beams were generated in 3D free space. An intuitive extension of this unique wave packet to two dimensions would possibly forecast more fascinating physics and applications, especially as it is accommodated in the subwavelength plasmonics, which is another active field nowadays [11–15]. As has been envisioned theoretically [16], a plasmonic Airy beam would provide an effective means to route energy over a metal surface between plasmonic devices.

According the nature of the Airy wave packet [1], a $3/2$-power phase modulation along the lateral dimension of beam is required [17,18]. It is commonly modulated to the 3-power phase type by a mask on an incident Gaussian beam with a followed Fourier transformation in generations of free space Airy beams [2–10]. This phase requirement is inherited for a surface plasmon polariton (SPP) Airy beam with a modified field form [16]. However, the conventional method tends to be hardly adopted in the SPP regime due to the complex transformation process and large spatial expense. Although an alternative approach was conceived by coupling a free-space-generated Airy beam into a planar plasmonic one [16], it will inevitably bring other severe obstacles and remains a great inconvenience in the full in-plane manipulations.

Here, we report a new experimental realization of plasmonic Airy beams on a silver surface at a visible wavelength, which is accomplished by particular diffraction processes with a carefully designed nanocave array on a metal surface. This achieved plasmonic Airy beam directly reveals the nonspreading, self-bending, and self-healing properties and demonstrates the capacity of a transversely self-confined SPP beam in a planar dimension with lower propagation loss. The proposed new diffraction approach by designable nanostructures has exhibited its flexibility in beam tailoring, which may significantly stimulate further manipulations of SPPs in a planar dimension.

Using a periodic array on metal surfaces to manipulate SPP propagations has achieved great success in recent years [19–22]. These approaches used to change the SPP propagations can also be interpreted as a phase modulation, which is in coincidence with the descriptions in diffraction optics. In principle, it is quite possible to use an inhomogeneous array to change a linear phase of an incident SPP into a nonlinear one. Therefore, the Airy beam requiring $3/2$ phase modulation is highly expected by diffractions in a nonperiodic array system. The scheme of our design is shown in Fig. 1. On the surface of a silver film (with $SiO_2$ as the substrate), an in-plane propagating SPP wave, generated by a grating coupling of a He-Ne laser ($\lambda_0 = 632.8$ nm), directly incidents into a nonperiodically arranged nanocave array. The diffracted SPP waves from nanocaves will interfere and ultimately build two SPP Airy beams on both sides.

In experiments, the nanocave array sample was fabricated by focused ion beam (FEI Strata FIB 201, 30 keV, 11 pA) milling on a 60-nm-thickness silver film, which has been deposited on a 0.2-mm-thickness $SiO_2$ substrate. The analysis of SPP wave propagation was performed by a home-built leakage radiation microscope (LRM) system [23,24] (for details, see [25]). The inset image in the lower right of Fig. 1 is a typical experimental result, which intuitively demonstrates the generation of SPP Airy beams that are very analogous to the schematic illustration, manifesting the self-bending, nonspreading, and multiple lobes. Here, the sample of the nanocave array is designed graded in the $x$ direction and periodic in the $z$ direction. Figure 2(a) depicts the top view of the graded nanocave

 

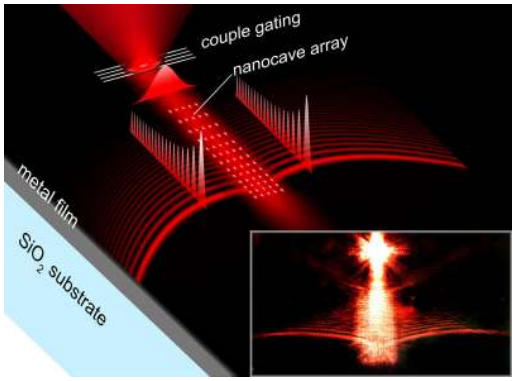


FIG. 1 (color online). Schematic of the generation of the SPP Airy beam. A laser beam is coupled into an in-plane propagating SPP wave by grating and incidents into a nonperiodically arranged nanocave array. Two SPP Airy beams are formed on both sides of the array by diffraction processes. The inset is a typical experimental result of a SPP Airy beam examined by the LRM system.

array together with a grating coupler, and the detected SPP beam in the right branch is specifically shown in Fig. 2(b), where a set of Airy-like wave profiles is clearly manifested. Subsequently, we performed a theoretical calculation based on the Huygens-Fresnel principle [18] that all nanocaves in the array are considered as subsources radiating cylindrical surface waves with designed initial phases. The calculated beam trajectories [shown in Fig. 2(c)] are in good agreement with the experiment ones, although they are both imperfect due to limited diffraction elements and nonideal modulations.

To explain how the SPP Airy-like beam comes into being, a nonlinear phase modulation by diffractions from a nonperiodic array is introduced. As is well known, an incident SPP wave will be diffracted into a well-defined direction by a designed array governed by the Bragg

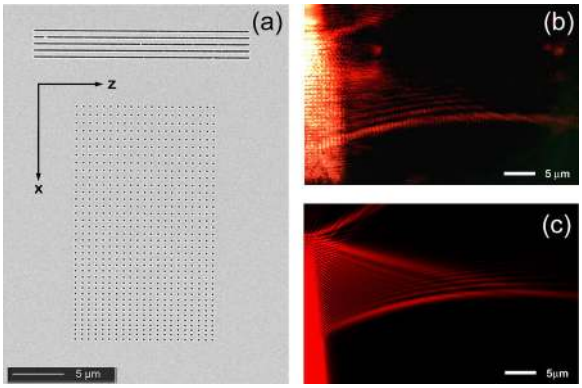


FIG. 2 (color online). (a) Top view of the graded nanocave array sample fabricated by a focused ion beam, where the lattice parameter is graded in the $x$ dimension ($a_x$ from 420 to 780 nm, grads $\Delta = 10$ nm), and the period in the $z$ dimension is $p_z = 620$ nm. (b) Experimentally achieved SPP beam trajectories and (c) the calculated one.

condition, which can be clearly schemed out in the reciprocal space [26] [see Fig. 3(a)]. However, if this condition is not perfectly satisfied, a preference diffraction will still occur with some sacrifice in intensity (as long as the deviation is not too large), owing to the elongated reciprocal lattice of the finite-scale array [see Fig. 3(b)] that is similar to the x-ray diffraction cases [27]. It is also proved by our experiments [28]. Therefore, a different lattice parameter is able to determine the preference diffraction direction, which can be regarded equivalently to yield an extra phase change of $2\pi$ from every local lattice (in the $x$ direction). When a graded array is employed, the incident beam will diffract to different directions at different positions according to the local lattice parameters (for this small gradient case, $\Delta = 10$ nm). Thus, we can obtain the corresponding phase evolution from every lattice point in the incident SPP propagation ($x$ direction) as $\phi(x) = \phi_0 + k_{\mathrm{spp}}x - 2m\pi$. This phase evolution in turn manifests the gradually changed diffraction directions by the graded lattice.

From Fig. 2(a), a beaming angle ($\theta \sim 20°$) with respect to the $z$ axis is found for the main lobe. This means that the lattice boundary (line $z = 0$) is not the start line of this SPP Airy beam. We can deduce the phase information at a virtual starting line in the $\xi$ axis that is perpendicular to the tangent of the beaming trajectory of the main lobe according to the principle of geometric optics as [see the scheme in Fig. 3(c)]

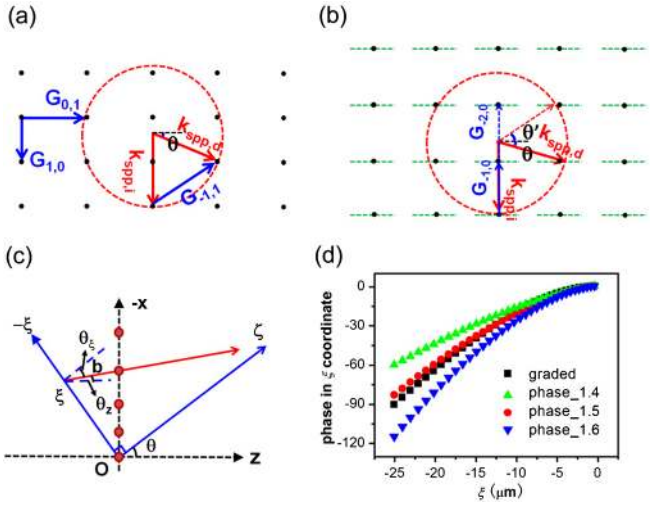


FIG. 3 (color online). Ewald construction for SPP diffraction direction with the Bragg condition is (a) satisfied and (b) not perfectly satisfied with limit diffraction elements in the $z$ axis (elongated reciprocal lattices in the $z$ axis are indicated). $k_{\mathrm{spp},i}$ and $k_{\mathrm{spp},d}$ are the incident and diffracted SPP wave vectors, respectively. $G_{0,1}$ and $G_{1,0}$ are two basic vectors of the reciprocal lattice. (c) Scheme of the phase transformation from the $x$ axis to a virtual $\xi$ axis, which can be designed with respect to the beaming angle $\theta$ for the main lobe of the SPP Airy beam. (d) Deduced phase distributions in the starting $\xi$ axis together with the 1.4-, 1.5-, and 1.6-power phase modulations.

$$\phi(\xi) = \phi(x) - k_{\mathrm{spp}} b = 2m\pi + k_{\mathrm{spp}} x - k_{\mathrm{spp}} b, \quad (1)$$

where

$$b = -\frac{x\tan(\theta_0)}{\cos(\theta_x) + \tan(\theta_0)\sin(\theta_x)}, \qquad \xi = \frac{x}{\cos(\theta_0)[1 + \tan(\theta_x)\tan(\theta_0)]}, \quad (2)$$

and $\sin(\theta_0) = \frac{\lambda_{\mathrm{spp}} - a_0}{a_0}$, $\sin(\theta_x) = \frac{\lambda_{\mathrm{spp}} - a_x}{a_x}$, and $a_x$ is defined as the local lattice determined by the mean value of two distances before and after the lattice of $x$. According to the experimental result of the position of the original point of $O$ ($a_0 \sim 450$ nm) and initial angle ($\theta \sim 20°$), we calculated the transformed phase $\phi(\xi)$ shown in Fig. 3(d) together with the results of 1.4-, 1.5-, and 1.6-power phase modulations. It is clearly seen that the deduced data from the graded array match the 3/2-power relation well, explaining the outcome of the Airy-like SPP beam.

Based on the above phase modulation method, a SPP Airy beam with a defined beaming direction can be generated by a proper nonperiodic array. With a given angle of $\theta$, the corresponding phase along the $x$ axis can be retrieved as

$$\psi(x) = -\frac{2}{3}\left(-\frac{\xi}{\xi_0}\right)^{3/2} - \frac{\pi}{4} - k\frac{\xi\sin\theta}{\cos(\theta - \theta_\xi)}, \quad (3)$$

where $x = \xi\cos(\theta) + \xi\sin(\theta)\tan(\theta - \theta_\xi)$, $\theta_\xi = \arcsin[\partial_\xi \phi(\xi)]$, $\phi(\xi)$ is the phase satisfying the Airy function, and $\xi_0$ is a constant that determines the acceleration of Airy beam. According to the equivalent phase by diffraction $\phi_m(x) = kx + 2m\pi$, we can deduce the location of the $m$th diffraction unit by solving $\phi_m(x) = \psi(x)$ and ultimately retrieve the arrangement of the nanocave array. Figure 4(a) is the calculated SPP beam trajectories constructed by the diffraction processes with the designed array data shown in the inset image ($p_z = 640$ nm), corresponding to a horizontal beaming of $\theta = 0°$ with $\xi_0 = 1.08$. Figure 4(b) is the experimental result recorded by the LRM system, which well reproduces the calculated one, indicating the outcome of the SPP Airy beam. The inset image is the distribution of field intensity in the $x$ axis picked up from the line of $z = 15$ $\mu$m (15 $\mu$m away from the start line), in which a definite Airy-like profile and small FWHM $\sim 1.3$ $\mu$m of the main lobe are clearly manifested. Similar to the previous result [Fig. 2(b)], this main lobe exhibits a weaker attenuation and preserves its narrow beam width over a long distance [28].

In the following, we would like to make a detailed analysis on the propagation property of this achieved SPP Airy beam. Figure 5(a) depicts the normalized field intensity of the main lobe as a function of propagation distance with a comparison to that of a conventional SPP Gaussian beam, where the inset shows the directly coupled SPP

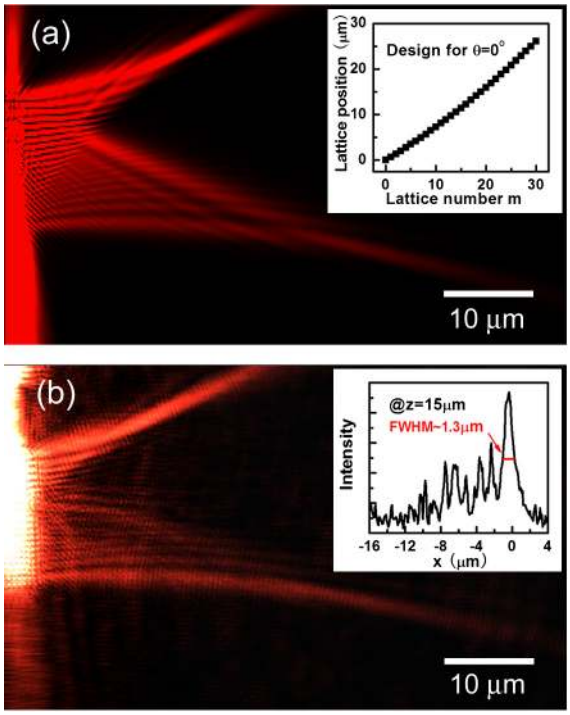


FIG. 4 (color online). (a) Theoretically calculated SPP propagation trajectories corresponding to a horizontal beaming ($\theta = 0°$) with a designed nonperiodic lattice in the $x$ dimension (inset image) and $p_z = 640$ nm ($\xi_0 = 1.08$). (b) Experimentally recorded SPP beam trajectories by the LRM system with a beam profile at the propagation distance of $z = 15$ $\mu$m (inset image), for example.

Gaussian beam recorded by LRM (with an initial FWHM $\sim 3$ $\mu$m). It is well demonstrated that the Airy beam has a much longer propagation length ($\sim 50$ $\mu$m) than the Gaussian beam ($\sim 15$ $\mu$m). Considering the narrow beam width, the main lobe of the SPP Airy beam behaves like a self-confined in-plane waveguide with lower loss and suggests possible applications in guiding SPP waves. To further confirm the characteristics of the Airy beam, we plot the trajectory of the main lobe, which shows considerable coincidence with the analytical parabolic curve derived from our design; see Fig. 5(b). In addition, we artificially introduced two blocks in the beam paths to test the self-healing property, as shown in Figs. 5(c) and 5(d) for blocks of small ($1.5 \times 0.6$ $\mu$m$^2$) and large ($2.2 \times 0.6$ $\mu$m$^2$) rectangular holes, respectively. It is evident that the SPP Airy beams indeed heal up by themselves for both cases. Therefore, it is not doubted that a well-developed SPP Airy beam is accomplished in a designable way.

For further discussions, one point should be addressed that the beam width of main lobe ($\sim 1.3$ $\mu$m) is near to the SPP wavelength ($\lambda_{\mathrm{SPP}} = 610$ nm) and the constant $\xi_0 = 1.08$ in Eq. (3) is not large enough considering the paraxial condition [29]. But it is still valid since such a SPP Airy beam still has a long dispersive distance (larger than

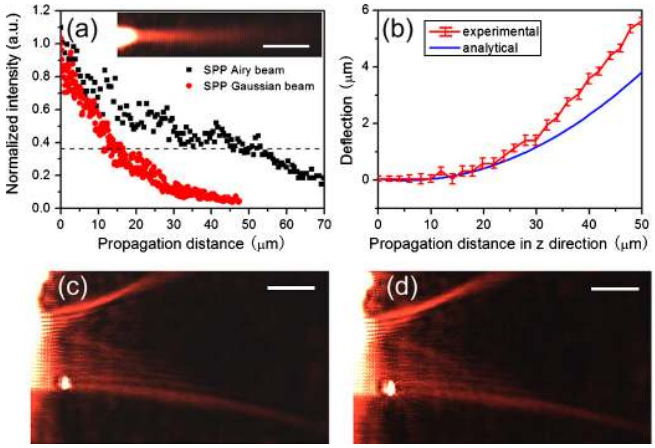


FIG. 5 (color online). (a) Field intensities of the main lobe of the SPP Airy beam and a conventional Gaussian beam as functions of propagation distance. The inset image is the LRM-detected Gaussian beam (initial FWHM $\sim 3$ $\mu$m). (b) Experimental trajectory of the main lobe compared with the analytical parabolic curve for the case of horizontal beaming. Experimental results of self-healing with respect to (c) a small rectangular block ($1.5 \times 0.6$ $\mu m^2$) and (d) a larger one ($2.2 \times 0.6$ $\mu m^2$). All scale bars equal 10 $\mu$m.

70 $\mu$m for the main lobe) [28]. From our additional simulations, if $\xi_0$ is further decreased, the Airy beam will disperse in a shorter distance and tend to totally collapse. Besides, in our approach the exact intensity modulation of the initial Airy function (the $-1/4$-power relation [1]) is not completely fulfilled. Fortunately, the graded system is able to build a localized wave packet at its propagation end (around the matched condition) [30], which usually has an asymmetric profile that is considerably analogous to the intensity envelope required by the Airy function. As for a more precise intensity modulation, we believe the beam would be improved by carefully tuning the diffraction elements. The phase modulation is the critical factor to achieve the Airy beam [17,18], and it is well proved to be fulfilled by such in-plane diffraction processes.

In conclusion, we have experimentally demonstrated the SPP Airy beam on a silver surface by particularly designed in-plane diffraction processes. The revealed SPP Airy beam exhibits unique features as expected, and the nonspreading property with lateral confinement for the main lobe over a long distance has implications in SPP manipulation and other related fields (e.g., arranging nanoparticles in nanoscale). Notably, the newly proposed method based on the nonperfectly matched diffraction effect allows for flexible modulations on the established plasmonic Airy beam almost at will, which may have more general applications in the wave-front tailoring as well as developing new kinds of photonic or plasmonic devices.

This work is supported by the State Key Program for Basic Research of China (No. 2012CB921501, No. 2009CB930501, and No. 2011CBA00200) and the National Natural Science Foundation of China (No. 11174136, No. 10974090, No. 60990320, and No. 11021403).

*Corresponding author.
taoli@nju.edu.cn
†http://dsl.nju.edu.cn/litao

[1] M. V. Berry and N. L. Balazs, Am. J. Phys. **47**, 264 (1979).
[2] G. A. Siviloglou, J. Broky, A. Dogariu, and D. N. Christodoulides, Phys. Rev. Lett. **99**, 213901 (2007).
[3] G. A. Siviloglou, and D. N. Christodoulides, Opt. Lett. **32**, 979 (2007).
[4] G. A. Siviloglou, J. Broky, A. Dogariu, and D. N. Christodoulides, Opt. Lett. **33**, 207 (2008).
[5] J. Broky, G. A. Siviloglou, A. Dogariu, and D. N. Christodoulides, Opt. Express **16**, 12 880 (2008).
[6] L. Carretero *et al.*, Opt. Express **17**, 22 432 (2009).
[7] T. Ellenbogen, N. Voloch-Bloch, A. Ganany-Padowicz, and A. Arie, Nat. Photon. **3**, 395 (2009).
[8] J. Baumgartl, M. Mazilu, and K. Dholakia, Nat. Photon. **2**, 675 (2008).
[9] P. Polynkin, M. Kolesik, J. V. Moloney, G. A. Siviloglou, and D. N. Christodoulides, Science **324**, 229 (2009).
[10] Y. L. Gu and G. Gbur, Opt. Lett. **35**, 3456 (2010).
[11] E. Ozbay, Science **311**, 189 (2006).
[12] D. K. Gramotnev and S. I. Bozhevolnyi, Nat. Photon. **4**, 83 (2010).
[13] W. L. Barnes, A. Dereux, and T. W. Ebbesen, Nature (London) **424**, 824 (2003).
[14] H. Ditlbacher, J. R. Krenn, G. Schider, A. Leitner, and F. R. Aussenegg, Appl. Phys. Lett. **81**, 1762 (2002).
[15] I. P. Radko *et al.*, Laser Photon. Rev. **3**, 575 (2009).
[16] A. Salandrino and D. N. Christodoulides, Opt. Lett. **35**, 2082 (2010).
[17] D. M. Cottrell, J. A. Davis, and T. M. Hazard, Opt. Lett. **34**, 2634 (2009).
[18] Y. Kaganovsky and E. Heyman, Opt. Express **18**, 8440 (2010).
[19] L. L. Yin *et al.*, Nano Lett. **5**, 1399 (2005).
[20] M. U. González *et al.*, Phys. Rev. B **73**, 155416 (2006).
[21] A. B. Evlyukhin, S. I. Bozhevolnyi, A. L. Stepanov, and J. R. Krenn, Appl. Phys. B **84**, 29 (2006).
[22] A. Drezet *et al.*, Nano Lett. **7**, 1697 (2007).
[23] A. Drezet *et al.*, Mater. Sci. Eng. B **149**, 220 (2008).
[24] A. Drezet *et al.*, Appl. Phys. Lett. **89**, 091117 (2006).
[25] A microscope objective ($50\times$, NA $= 0.55$) is used to focus the incident He-Ne laser, and another oil immersion objective ($160\times$, NA $= 1.40$) is used to collect the leakage radiation.
[26] A.-L. Baudrion *et al.*, Phys. Rev. B **74**, 125406 (2006).
[27] A. Guinier, *X-Ray Diffraction* (Freeman, London, 1963).
[28] See Supplemental Material at http://link.aps.org/supplemental/10.1103/PhysRevLett.107.126804 for preference diffraction, SPP Airy beam width, and paraxiality.
[29] A. V. Novistsky and D. V. Novitsky, Opt. Lett. **34**, 3430 (2009).
[30] S. M. Wang *et al.*, Appl. Phys. Lett. **93**, 233102 (2008).